Quadrupole moments of odd-A $^{53-63}$Mn: Onset of collectivity towards N = 40

DOI:
10.1016/j.physletb.2016.07.016

Document Version
Final published version

Published in:
Physics Letters. Section B: Nuclear, Elementary Particle and High-Energy Physics

Physics Letters B 760 (2016) 387–392

Contents lists available at ScienceDirect

Physics Letters B

www.elsevier.com/locate/physletb

Quadrupole moments of odd-A $^{53-63}$Mn: Onset of collectivity towards $N = 40$

C. Babcock [a,b,*], H. Heylen [c,*], M.L. Bissell [d], K. Blaum [e], P. Campbell [d], B. Cheal [a], D. Fedorov [k], R.F. Garcia Ruiz [c], W. Geithner [g], W. Gins [c], T. Day Goodacre [d,b], L.K. Grob [i,d], M. Kowalska [b], S.M. Lenzi [h], B. Maass [i], S. Malbrunot-Ettenauer [b], B. Marsh [b], R. Neugart [e,j], G. Neyens [c], W. Nörtershäuser [i], T. Otsuka [f], R. Rossel [b], S. Rothe [b], R. Sánchez [g], Y. Tsunoda [l], C. Wraith [a], L. Xie [d], X.F. Yang [c]

[a] Oliver Lodge Laboratory, Oxford Street, University of Liverpool, L69 7ZE, UK
[b] ISOLDE, CERN, CH-1211 Geneva 23, Switzerland
[c] KU Leuven, Instituut voor Kern- en Stralingsfysica, 3001 Leuven, Belgium
[d] School of Physics and Astronomy, University of Manchester, M13 9PL, UK
[e] Max-Plank-Institut für Kernphysik, D-69117 Heidelberg, Germany
[f] Dept. of Physics, University of Tokyo, Hongo, Bunkyo-ku, Tokyo 113-0033, Japan
[g] GSI Helmholtzzentrum für Schwerionenforschung GmbH, D-64291 Darmstadt, Germany
[h] Dipartimento di Fisica e Astronomia dell'Università and INFN, Sezione di Padova, I-35131 Padova, Italy
[i] Institut für Kernphysik, TU Darmstadt, D-64289 Darmstadt, Germany
[j] Institut für Kernchemie, Johannes Gutenberg-Universität Mainz, D-55128, Germany
[k] Petersburg Nuclear Physics Institute, 188350 Gatchina, Russia
[l] Center for Nuclear Study, University of Tokyo, Hongo, Bunkyo-ku, Tokyo 113-0033, Japan

ARTICLE INFO

Article history:
Received 20 March 2016
Received in revised form 23 June 2016
Accepted 6 July 2016
Available online 12 July 2016
Editor: D.F. Geesaman

Keywords:
Quadrupole moments
Laser spectroscopy
Manganese
Deformation
Optical pumping

ABSTRACT

The spectroscopic quadrupole moments of the odd–even Mn isotopes between $N = 28$ and $N = 38$ have been measured using bunched-beam collinear laser spectroscopy at ISOLDE, CERN. In order to increase sensitivity to the quadrupole interaction, the measurements have been done using a transition in the ion rather than in the atom, with the additional advantage of better spectroscopic efficiency. Since the chosen transition is from a metastable state, optical pumping in ISOLDE's cooler and buncher (ISCOOL) was used to populate this state. The extracted quadrupole moments are compared to large-scale shell model predictions using three effective interactions, GXPF1A, LNPS and modified A3DA. The inclusion of both the $1\nu g_{9/2}$ and $2\nu d_{5/2}$ orbitals in the model space is shown to be necessary to reproduce the observed increase in the quadrupole deformation from $N = 36$ onwards. Specifically, the inclusion of the $2\nu d_{5/2}$ orbital induces an increase in neutron and proton excitations across the reduced gaps at $N = 40$ and $Z = 28$, leading to an increase in deformation above $N = 36$.

1. Introduction

The region around $N = 40$ has been extensively studied in recent years due to the sudden changes in nuclear structure observed below $^{68}_{28}$Ni$_{40}$. The neutron-rich manganese isotopes studied here ($Z = 25$) provide an opportunity to investigate shell structure evolution towards this weak subshell closure [1,2]. In the neighboring elements of Cr ($Z = 24$) and Fe ($Z = 26$), the electromagnetic transition probabilities and level structures have been studied in several works and evidence has been found for deformation in their neutron-rich isotopes. In Fe, the onset of collectivity is found at ^{64}Fe$_{38}$ [1] and this collectivity persists in more neutron-rich isotopes, as demonstrated by $B(E2)$ values [3,4], the decreased energy of the 2^+_1 state in ^{66}Fe$_{40}$ [5] and the $E(4^+)/E(2^+)$ ratio systematics [6]. From the measured $B(E2)$ values, a deformation parameter of $\beta \approx 0.28$ is found for ^{64,66}Fe$_{38,40}$ [3].

In Cr, the isotopes between ^{56}Cr$_{32}$ and ^{60}Cr$_{36}$ begin to show an enhancement in collectivity, demonstrated by an energy level structure characteristic of the transition from vibrational exci-

* Corresponding authors.
E-mail addresses: cbabcock@cern.ch (C. Babcock), hanne.heylen@fys.kuleuven.be (H. Heylen).

http://dx.doi.org/10.1016/j.physletb.2016.07.016

tation to rotational collectivity [7]. From $^{62}Cr_{38}$ onwards, the $E(4^+)/E(2^+)$ ratios suggest a more rotational character, providing evidence for static prolate deformation in the heavier isotopes [6,8], and a deformation parameter of $\beta \approx 0.35$ has been reported for $^{62}Cr_{38}$ [1]. The emerging picture of increased quadrupole collectivity is further supported by the $B(E2)$ values up to $N = 40$ [4,9]. More recently however, theoretical calculations have suggested that the low-lying states of neutron-rich Cr cannot be characterized as strictly prolate rigid-rotor and should instead be understood as dominated by large amplitude shape fluctuations [10].

Mass measurements of Cr and Fe isotopes indicate a weak $N = 40$ gap [11–13], making occupation of the $\nu g_{9/2}$ and $\nu d_{5/2}$ orbitals energetically favorable. The promotion of neutrons to the $g_{9/2}$ orbital has been proposed as a driver of deformation [8,14]. Similarly, the $\nu d_{5/2}$ orbital may play an important role in the development of quadrupole collectivity for isotopes closer to $N = 40$ [1,15], however the specific role of excitations to this orbital remains ambiguous. While some calculations in this mass region are limited to the $fpg_{9/2}$ orbitals [2,16], the $\nu d_{5/2}$ has an important influence on the development of quadrupole correlations, and hence deformation, in the quasi-SU(3) picture [17].

The development of collectivity is correlated not only to the excitation of neutrons across $N = 40$, but to the dimensions of the total proton-neutron valence space of a particular isotope [3]. It is therefore not surprising that the degree of collectivity in these open $\pi f_{7/2}$ nuclei is largest for the mid-shell Cr isotopes.

The observations of Fe and Cr suggest that we may expect to see a similar increase in collectivity in their odd-proton neighbor, Mn ($Z = 25$) [7]. Indeed, a quasi-collective band may have been observed for $^{57-60}Mn_{32-35}$ [18] and the unexpectedly long beta-decay half-lives in $N \simeq 40$ Mn isotopes are suggested to be the result of the preferential filling of the positive parity $\nu g_{9/2}$ orbital which can only decay through forbidden transitions [5]. In order to investigate the degree of collectivity in the Mn isotopes and the role played by the $\nu d_{5/2}$ orbital, the spectroscopic quadrupole moment can serve as a direct probe. This observable is, in principle, directly obtainable from the hyperfine structure measured with high-resolution laser spectroscopy in a model-independent way.

Previous laser spectroscopy studies of atomic Mn were not successful in measuring precise quadrupole moments for the neutron-rich isotopes due to the small quadrupole splitting of the atomic ground state and the chosen excited levels [19,20]. An excited state in the Mn ion at 43370.51 cm^{-1} is known to have larger quadrupole splitting [21], however the transition to this level from the ionic ground state is spectroscopically weak. A more suitable transition for spectroscopy exists between a metastable ionic state and the excited state, however the natural population of the metastable state after the ion production process is too low to efficiently perform spectroscopy. Optical pumping has therefore been used to enhance the population of the metastable state [21,22].

Here, the technique of optical pumping is used in ISOLDE's cooler/buncher ion trap for the first time to enable the quadrupole moments of neutron-rich odd–even ionic manganese isotopes to be measured.

2. Experimental method

The experiment was performed at ISOLDE [23], CERN, where the manganese ions were produced by bombarding a uranium carbide target with a 1.4 GeV proton beam. After diffusing from the target, the reaction products of interest were ionized using the Resonance Ionization Laser Ion Source (RILIS) [24], then extracted and passed through the two mass-separating dipole magnets of the High Resolution Separator (HRS). They were then collected in ISCOOL, ISOLDE's radio frequency quadrupole cooler and buncher [25], which decelerates and cools the ions then traps the cooled ions in a potential well. While they were trapped in the potential well, the ions were optically pumped into the metastable state by resonant laser excitation and decay, using an additional pulsed laser from the RILIS laser lab. The optical pumping laser beam entered the second separator magnet via a quartz window, then passed through the separator magnet and the injection apertures of ISCOOL to interact with the trapped ion bunch near the extraction region, as shown in Fig. 1.

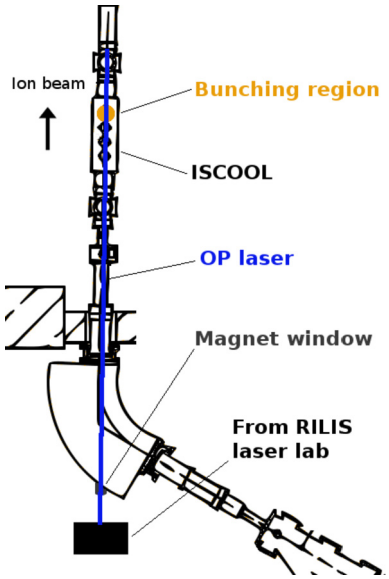

Fig. 1. Schematic for the entry of optical pumping (OP) lasers from the RILIS laser lab into the cooler/buncher (ISCOOL), where they interact with trapped ions in the bunching region (color online).

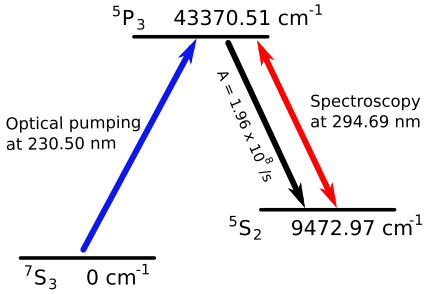

Fig. 2. Optical pumping scheme used to excite trapped manganese ions from the ground state to a low-lying metastable state at 9472.97 cm^{-1} via an intermediate excited state (color online).

The optical pumping scheme is shown in Fig. 2. A pulsed laser beam with a repetition rate of 10 kHz was produced by a frequency quadrupled titanium sapphire laser at 230.50 nm. The broadband 10 GHz laser linewidth was well matched to the Doppler broadened profile of the ions in the trap. The ions were first excited from the $^7S_3$ ground state to the $^5P_3$ state at 43 370.51 cm^{-1}. The relatively weak transition strength ($A_{ki} = 1.55 \times 10^6$ s^{-1} [26]) is offset by the extended trapping time in the cooler/buncher (200 ms), which allowed multiple laser-ion interactions to take place, even with moderate laser power. From the excited state, the ions decay with a branching ratio of 0.8 to the $^5S_2$ level at 9472.97 cm^{-1}. The decay from the $^5S_2$ metastable state to the ground state is a forbidden transition, so with increasing laser interaction time, the population of ions in the metastable state accumulates. Any effects of collisional de-excitation were balanced

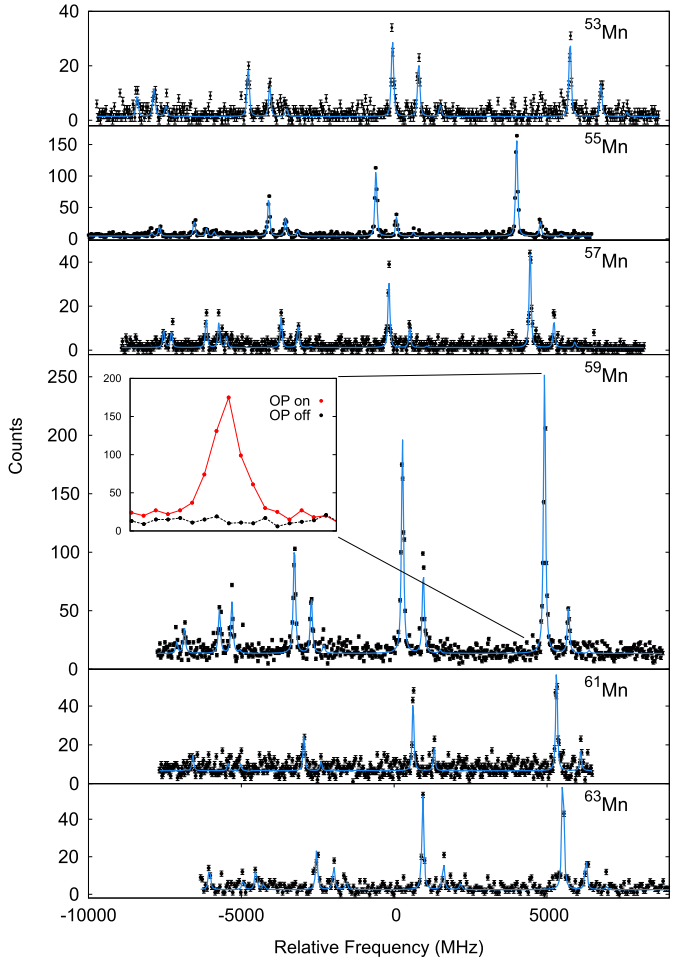

Fig. 3. Example spectra for the odd–even isotopes $^{53-63}$Mn, with the fits overlaid. The inset shows one peak of ^{59}Mn with the optical pumping (OP) laser on and off. The frequency is plotted relative to the ^{55}Mn centroid (color online).

by the repeated laser-ion interactions, and thus did not affect the population of the final state.

The optically pumped ions were subsequently released in bunches of approximately 4 μs length and directed to the COLLAPS setup [27] for investigation via collinear laser spectroscopy. The beam was overlapped with co-propagating light from a frequency-doubled narrowband dye laser that provided approximately 1 mW of power at a Doppler-shifted vacuum wavelength of 294.69 nm, in order to probe the transition from the metastable state described above. A tuning voltage applied to the interaction region modulated the energy of the bunch from its initial 30 keV, thus effectively Doppler shifting the laser frequency seen by the ions over the range of the hyperfine splitting. Four photomultiplier tubes surrounded the interaction region of the setup and detected the emitted fluorescence as the ions decayed back to the metastable state. The background due to dark counts and randomly scattered laser light was reduced by a factor of approximately 10^4 by restricting the data acquisition system to accept photomultiplier counts only during the time that the ion bunch traversed the interaction region [28–30]. In the case of ^{63}Mn, photons were only accepted within one half-life (275 ms) after the proton pulse on target (a method called proton triggering, see [20] for details) in order to further suppress the background counts. A total experimental efficiency gain of approximately an order of magnitude was observed with respect to our previous measurement using atomic manganese [19]. In addition to the increased sensitivity to the quadrupole interaction provided by the chosen transition, ionic transitions have the advantage that they do not suffer from the problem of populating a large number of states during the charge-exchange process, as is the case in the atom. Despite lower yields resulting from problems with the ISOLDE target, these advantages enabled a successful investigation of isotopes up to ^{63}Mn.

Table 1
The hyperfine A and B values of the upper ($^5P_3$) and lower ($^5S_2$) states extracted in this experiment (the $B(^5S_2)$ values were approximately 0 MHz for all isotopes). Statistical errors, which dominate the uncertainty, are shown.

Isotope	$A(^5P_3)$ (MHz)	$B(^5P_3)$ (MHz)	$A(^5S_2)$ (MHz)
^{53}Mn	−156.2(9)	+16(13)	−1239.4(13)
^{55}Mn	−150.1(2)	+86(3)	−1195.3(4)
^{57}Mn	−151.3(5)	+95(6)	−1201.1(7)
^{59}Mn	−151.2(7)	+90(9)	−1204.9(9)
^{61}Mn	−153.5(4)	+95(5)	−1218.2(6)
^{63}Mn	−149.7(5)	+124(7)	−1185.8(9)

The hyperfine spectra collected in this way were fitted with Voigt line profiles and unconstrained intensities, using a least-squares method as outlined in [28]. The known nuclear spins [19] were used to extract the A and B coefficients of the hyperfine structure [28–30].

Fig. 3 shows example spectra for all six isotopes measured. Without the use of optical pumping, no resonant counts were seen.

3. Results

The extracted A and B coefficients of the hyperfine spectra for the $^5P_3$ and $^5S_2$ states are shown in Table 1. The A and B coefficients for ^{53,55}Mn have been measured previously in a similar optical pumping experiment for neutron-deficient isotopes [21], and the results shown here agree to within 2σ. Table 2 shows the magnetic dipole moments extracted from the $A(^5P_3)$ state and the spectroscopic quadrupole moments extracted from the $B(^5S_2)$ state using the relations [28,30],

$$\mu = \mu_{\text{ref}} \frac{IA}{I_{\text{ref}} A_{\text{ref}}} \tag{1}$$

$$Q_s = Q_{\text{ref}} \frac{B}{B_{\text{ref}}} \tag{2}$$

where the reference values are those of ^{55}Mn listed in Table 2. The hyperfine anomaly was assumed to be negligible. The dipole moments show good agreement with those previously measured for atomic Mn [19].

4. Discussion

Comparison of experimental data to theoretical calculations is a powerful method for testing our current understanding of nuclear structure and dynamics across the nuclear chart. In particular, regions of rapid structural change, such as those around $N = 40$, pose serious challenges.

Fig. 4 and Table 2 show a comparison of the experimental quadrupole moments with the results of large-scale shell model calculations, performed using three different effective interactions and model spaces. The GXPF1A effective interaction [31] uses a ^{40}Ca core and is restricted to the pf space for both protons and neutrons. For computational reasons, a maximum of 2 protons and 6 neutrons can be excited across $Z = N = 28$. The LNPS interaction [17] uses a ^{48}Ca core and considers the entire pf shell for protons, and the $p_{3/2}$, $f_{5/2}$, $p_{1/2}$, $g_{9/2}$ and $d_{5/2}$ orbitals for neutrons. A maximum of 11 excitations across $Z = 28$ and $N = 40$ are allowed. The modified A3DA interaction [32] considers the

Table 2
The magnetic dipole and electric quadrupole moments derived from the coefficients in Table 1. The spin assignments have already been confirmed [19]. Also shown are the quadrupole moments calculated using the GXPF1A [31], LNPS [17] and modified A3DA [32] effective interactions. All calculations are done with effective charges $e_\pi = 1.31$ and $e_\nu = 0.46$.

Isotope	N	I	μ (μ_N)	Q_s (b)	Q_s (b) [GXPF1A]	Q_s (b) [LNPS]	Q_s (b) [modified A3DA]
^{53}Mn	28	7/2	+5.036(5)	+0.06(5)	+0.08	–	+0.08
^{55}Mn	30	5/2	+3.46871790(9)[a]	+0.33(1)[b]	+0.33	–	+0.33
^{57}Mn	32	5/2	+3.485(2)	+0.37(3)	+0.33	+0.31	+0.35
^{59}Mn	34	5/2	+3.496(3)	+0.34(4)	+0.31	+0.32	+0.32
^{61}Mn	36	5/2	+3.535(2)	+0.36(3)	+0.30	+0.35	+0.38
^{63}Mn	38	5/2	+3.441(3)	+0.48(4)	+0.26	+0.41	+0.41

[a] Reference from [33] with corrections for diamagnetic shielding.
[b] Reference from [34].

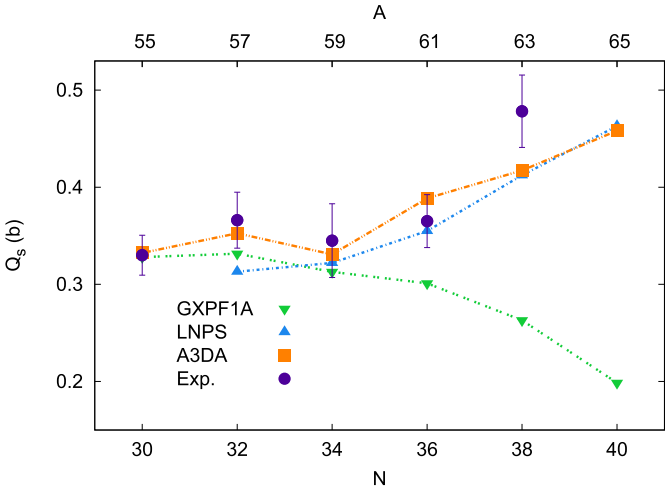

Fig. 4. Comparison of the quadrupole moments determined in this work to the results of calculations using the GXPF1A, LNPS, and modified A3DA effective interactions with $e_\pi = 1.31$ and $e_\nu = 0.46$ (color online).

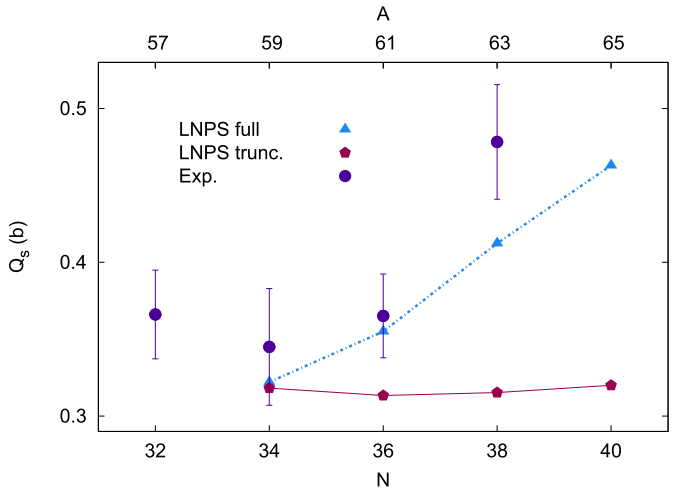

Fig. 5. The results of LNPS calculations of the quadrupole moment with neutron excitations limited to the $fpg_{9/2}$ space (labeled *trunc.*) and in the full $fpg_{9/2}d_{5/2}$ space (labeled *full*) are shown compared to experimental values (color online).

$fpg_{9/2}d_{5/2}$ space for protons and neutrons with ^{40}Ca as a core, and was able to include a larger model space by performing calculations in the Monte Carlo shell model framework [32]. Both the GXPF1A and LNPS calculations have been done using the ANTOINE shell model code [35], which imposes some computational limits on the size of the model space since a full Lanczos diagonalization is performed.

As can be seen in Fig. 4, the GXPF1A effective interaction successfully predicts the quadrupole moments up to ^{59}Mn ($N = 34$), after which the predictions and experimental data begin to diverge. The data follows an upward trend in deformation, as predicted by LNPS and modified A3DA, while the GXPF1A calculations follow a downward trend, as would be expected if there was a subshell gap at $N = 40$. Indeed, previous work on the magnetic moments [19,20] and energy levels [18] has demonstrated that the GXPF1A model space, which does not permit excitations across $N = 40$, is too limited to accurately describe the more neutron-rich Mn isotopes. Thus the larger model spaces employed by the LNPS and modified A3DA interactions are necessary to reproduce the experimental data. Both interactions have proven to be successful in this region of the nuclear chart [19,20,36,37], and LNPS has recently been used to accurately characterize a similar deformation trend in ^{58,60,62}Cr$_{34,36,38}$ [38].

Quadrupole moments are a useful tool to investigate the role of excitations across $N = 40$ because of their sensitivity to 2p-2h and 4p-4h excitations, and to the strength of the quadrupole collectivity. In particular, the quadrupole moments will be used to probe the role of the $\nu d_{5/2}$ orbital in the development of this collectivity. For this purpose, calculations of the theoretical quadrupole moments have been performed using LNPS in a truncated model space which excludes the $\nu d_{5/2}$ orbital. Fig. 5 shows the results of these calculations (labeled *trunc.*), where excitations have been limited to the $\nu g_{9/2}$ orbital. The quadrupole moments calculated this way do not reproduce the rising trend of the experimental data, but remain nearly constant from $N = 34$ onwards. The trend of the experimental data is only reproduced in the full $fpg_{9/2}d_{5/2}$ space. This demonstrates the necessity of including both the $\nu g_{9/2}$ and $\nu d_{5/2}$ orbitals in the model space – neutron excitations to $\nu g_{9/2}$ alone are not sufficient to explain the deformation in the Mn isotopes. This can be understood in terms of the pseudo and quasi SU(3) symmetry as discussed in [39].

The effect of the excitations across $N = 40$ can be seen more clearly in the occupation numbers of protons and neutrons for the upper pf and $g_{9/2}d_{5/2}$ orbitals. Fig. 6 shows a comparison of occupation numbers calculated using the LNPS interaction in the truncated $fpg_{9/2}$ space and the full $fpg_{9/2}d_{5/2}$ space.

The top panel of Fig. 6 shows that excitations to the $\nu g_{9/2}$ orbital are suppressed in the truncated $fpg_{9/2}$ space as compared to the $fpg_{9/2}d_{5/2}$ space. This illustrates the correlation between the increased occupation of the $\nu d_{5/2}$ orbital and the quadrupole collectivity, which also increases the excitations to the $\nu g_{9/2}$ orbital. The reduced neutron excitations across $N = 40$ in the $fpg_{9/2}$ space provide a possible explanation for the difference in predicted deformation, as shown in Fig. 5.

The exclusion of the $\nu d_{5/2}$ orbital also has consequences for proton excitations across $Z = 28$. The lower panel in Fig. 6 shows the proton excitations into the upper pf orbitals for both the $fpg_{9/2}$ and $fpg_{9/2}d_{5/2}$ spaces. While the total upper πpf shell oc-

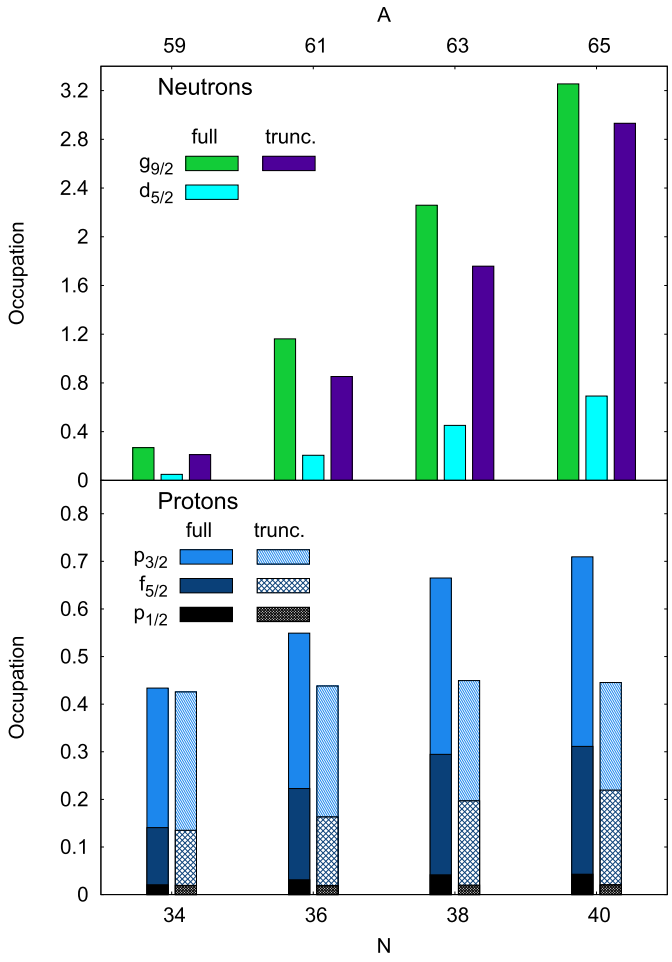

Fig. 6. Orbital occupation numbers for excitations past $N = 40$ and $Z = 28$. The labels *full* and *trunc.* refer to calculations done in the $fpg_{9/2}d_{5/2}$ and $fpg_{9/2}$ spaces respectively (color online).

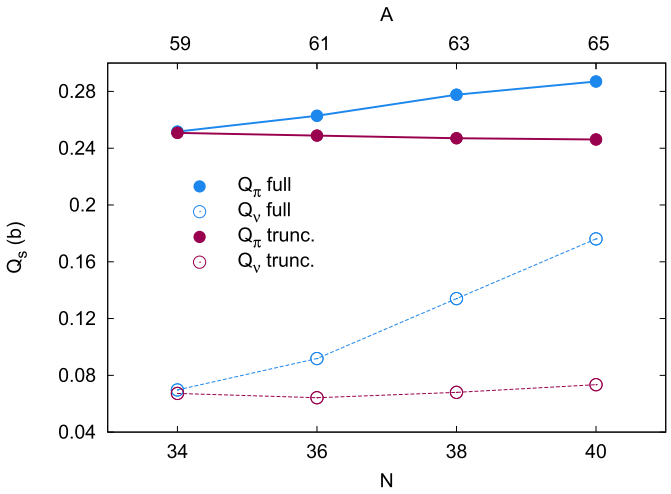

Fig. 7. Contribution of the neutrons and protons to the total quadrupole moment for both the $fpg_{9/2}$ and $fpg_{9/2}d_{5/2}$ space, where the labels *full* and *trunc.* have been used to indicate the $fpg_{9/2}d_{5/2}$ and $fpg_{9/2}$ spaces respectively (color online).

cupation for the truncated $fpg_{9/2}$ space remains nearly constant, this same occupation rises in the full $fpg_{9/2}d_{5/2}$ space with increasing N.

Since the exclusion of the $\nu d_{5/2}$ orbital has a significant effect on both neutron and proton excitations, it is helpful to look at the separate neutron and proton contributions to the total quadrupole moment, by decomposing it into its components, $Q = Q_\pi + Q_\nu$. The results for both the full and truncated spaces are shown in Fig. 7. In the limited $fpg_{9/2}$ model space, both the neutron and proton contributions remain essentially constant, showing no increase in deformation towards $N = 40$. In contrast, both contributions rise with increasing N in the full model space. The contribution from neutron correlations dominates the overall increase in the quadrupole moments, although the protons also induce an increase of $\Delta Q_s = 0.035\,\mathrm{b}$ between $N = 34$ and $N = 40$. The increase in the experimentally observed quadrupole moments between $N = 36$ and $N = 38$ is due to a combination of the rise in the neutron and proton quadrupole components. The comparison between the $fpg_{9/2}$ and $fpg_{9/2}d_{5/2}$ spaces emphasizes the trend seen in the occupation numbers.

Calculations using the modified A3DA interaction (see Fig. 4) obtain results similar to those of LNPS for the quadrupole moments, as well as the neutron and proton occupation numbers. In addition, this interaction has been used to calculate the potential energy surfaces of the Mn ground states, and the minima of these plots have shown a progression from a near spherical shape in ^{53}Mn, towards increasing prolate deformation in the more neutron rich isotopes up to ^{65}Mn [40]. This deformation is, however, not rigid and there is evidence that shape fluctuations with triaxial components play a role in the ground state structure of manganese towards $N = 40$. Though the spectroscopic quadrupole moment is not sensitive to such fluctuations, the rising deformation with neutron number predicted by the potential energy surfaces mirrors the increasing deformation observed experimentally.

5. Conclusions

Optical pumping in the ISOLDE cooler/buncher has been successfully applied in order to enhance the population of ionic Mn in a chosen metastable state, which allowed efficient collinear laser spectroscopy to be performed on the neutron-rich isotopes. Hyperfine A and B coefficients were extracted and electric quadrupole moments were determined for the odd–even $^{53-63}$Mn isotopes. The theoretically predicted quadrupole moments were calculated using three shell model effective interactions, GXPF1A, LNPS and modified A3DA. In comparing the observed moments to those calculated with the shell model interactions, the influence of the $\nu g_{9/2}$ and $\nu d_{5/2}$ orbitals on the developing collectivity can clearly be seen in the deviation of the observed values from those predicted by GXPF1A. The larger model spaces used by LNPS and modified A3DA reproduce the trend of the quadrupole moments very well in the region approaching $N = 40$. Calculations done using LNPS in a truncated $fpg_{9/2}$ space (thus excluding the $\nu d_{5/2}$ orbital) shed some light on the roles played by the individual orbitals above $N = 40$. It is found that the increase of the quadrupole moments and thus the development of collectivity towards $N = 40$ can only be reproduced if both the $g_{9/2}$ and $d_{5/2}$ orbitals are included in the calculations. By comparing the neutron and proton occupation numbers for the full and truncated LNPS calculations, it is clear that the inclusion of the $\nu d_{5/2}$ orbital leads to an increase in both neutron and proton excitations. A calculation of the individual neutron and proton contributions to the spectroscopic quadrupole moment confirmed this interpretation and demonstrated the important role of the $\nu d_{5/2}$ orbital in producing the necessary neutron and proton excitations to reproduce the observed deformation in the neutron-rich Mn isotopes.

Acknowledgements

This work was supported by the Belgian Research Initiative on Exotic Nuclei (IAP-project P7/12), the FWO-Vlaanderen, GOA grants 10/010 and 15/010 from KU Leuven, BMBF (05P15RDICA), the Max-Planck Society, the Science and Technology Facilities Council, and the European Union's Seventh Framework Programme for Research and Technological Development under Grant Agreements ENSAR (No. 262010), CATHI (No. 264330), COFUND (No. 267194) and LA^{3}NET (289191). We would like to thank the ISOLDE technical group for their support and assistance.

References

[1] J. Ljungvall, et al., Phys. Rev. C 81 (2010) 061301.
[2] J.J. Valiente-Dobón, et al., Phys. Rev. C 78 (2008) 024302.
[3] W. Rother, et al., Phys. Rev. Lett. 106 (2011) 022502.
[4] H.L. Crawford, et al., Phys. Rev. Lett. 110 (2013) 242701.
[5] M. Hannawald, et al., Phys. Rev. Lett. 82 (1999) 1391.
[6] C. Santamaria, et al., Phys. Rev. Lett. 115 (2015) 192501.
[7] N. Aoi, et al., Nucl. Phys. A 805 (2008) 400c, INPC 2007 Proceedings of the 23rd International Nuclear Physics Conference.
[8] N. Aoi, et al., Phys. Rev. Lett. 102 (2009) 012502.
[9] T. Baugher, et al., Phys. Rev. C 86 (2012) 011305.
[10] K. Sato, et al., Phys. Rev. C 86 (2012) 024316.
[11] S. Rahaman, et al., Eur. Phys. J. A 34 (2007) 5.
[12] S. Naimi, et al., Phys. Rev. C 86 (2012) 014325.
[13] C. Guénaut, et al., Phys. Rev. C 75 (2007) 044303.
[14] N. Hoteling, et al., Phys. Rev. C 82 (2010) 044305.
[15] E. Caurier, F. Nowacki, A. Poves, Eur. Phys. J. A 15 (2002) 145.
[16] H. Jin, Y. Sun, K. Kaneko, S. Tazaki, Phys. Rev. C 87 (2013) 044327.
[17] S.M. Lenzi, F. Nowacki, A. Poves, K. Sieja, Phys. Rev. C 82 (2010) 054301.
[18] D. Steppenbeck, et al., Phys. Rev. C 81 (2010) 014305.
[19] C. Babcock, et al., Phys. Lett. B 750 (2015) 176.
[20] H. Heylen, et al., Phys. Rev. C 92 (2015) 044311.
[21] F. Charlwood, et al., Phys. Lett. B 690 (2010) 346.
[22] B. Cheal, et al., Phys. Rev. Lett. 102 (2009) 222501.
[23] E. Kugler, Hyperfine Interact. 129 (2000) 23.
[24] B. Marsh, et al., Hyperfine Interact. 196 (2010) 129.
[25] H. Frånberg, et al., Nucl. Instrum. Methods B 266 (2008) 4502.
[26] M. McNally (Ed.), Kurucz Database, vol. XXB, Trans. IAU, Kluwer, Dordrecht, 1988.
[27] J. Papuga, et al., Phys. Rev. C 90 (2014) 034321.
[28] B. Cheal, K. Flanagan, J. Phys. G, Nucl. Part. Phys. 37 (2010) 113101.
[29] K. Blaum, J. Dilling, W. Nörtershäuser, Phys. Scr. 2013 (2013) 014017.
[30] P. Campbell, I. Moore, M. Pearson, Prog. Part. Nucl. Phys. 86 (2016) 127.
[31] M. Honma, T. Otsuka, B.A. Brown, T. Mizusaki, Eur. Phys. J. A 25 (2005) 499.
[32] T. Otsuka, et al., Prog. Part. Nucl. Phys. 47 (2001) 319.
[33] O. Lutz, W. Steinkilberg, Z. Naturforsch. 29a (1974) 1467.
[34] J. Dembczyński, et al., Z. Phys. Hadrons Nucl. 291 (1979) 207.
[35] E. Caurier, F. Nowacki, Acta Phys. Pol. B 30 (1999) 705.
[36] E. Sahin, et al., Phys. Rev. C 91 (2015) 034302.
[37] Y. Tsunoda, et al., Phys. Rev. C 89 (2014) 031301.
[38] T. Braunroth, et al., Phys. Rev. C 92 (2015) 034306.
[39] A.P. Zuker, A. Poves, F. Nowacki, S.M. Lenzi, Phys. Rev. C 92 (2015) 024320.
[40] H. Heylen, et al., 2016, submitted to Phys. Rev. C.